EuroSun 2026

PYTHON-BASED DYNAMIC SIMULATION OF A PVT-HEAT PUMP SYSTEM: OPERATING-MODE ANALYSIS AND COMPARISON WITH AN AIR-SOURCE HEAT PUMP

Valentin Delachaux[1] (corresponding author), Laetitia Brottier[2], Mohamad Ali Jaafar[2], and Rachid Bennacer[1]

[1] *ENS Paris-Saclay, Université Paris-Saclay, Gif-sur-Yvette, France*

[2] *Dualsun, Marseille, France*

valentin.delac@pm.me

Summary

Unglazed photovoltaic-thermal (PVT) collectors can serve as the sole heat source of a brine/water heat pump, but the models published for such systems document their components too partially to be audited, and report performance averaged over the month or the year, hiding the conditions that decide it. This paper presents a fully-Python dynamic model of indirect-expansion PVT solar-assisted heat pump (IDX-PVT-SAHP) and air-source heat pump (ASHP) systems, with component models, manufacturer performance maps and automatic sizing rules fully disclosed and released as open source. Both are simulated on the same single-family house (SFH45, Strasbourg) at a 2-minute time step and compared in terms of evaporator-to-ambient temperature pinch and performance by operating mode. At the compressor boundary the PVT source is 9.9% better than the air source on daytime space heating and 8.5% on daytime hot water, but concedes an evaporator-to-ambient temperature pinch of −5.2 K at night, governed by sky temperature and wind. Since night-time space heating alone consumes 65% of the electricity, that daytime advantage may not be sufficient to outperform the air-source unit. Besides, the seasonal performance comparison depends on the electric consumption of the source-loop circulator the PVT field requires, and the frosting/defrosting penalty of the air-source unit. The contribution is an auditable open model, a diagnosis resolved by operating mode, and the design levers it exposes (PVT-loop pressure drop, hydraulics and control), not a verdict between the two solutions.

Keywords: photovoltaic-thermal collector, WISC, solar-assisted heat pump, dynamic simulation, seasonal performance factor, frosting, defrosting

Field of application: Sustainable Heating and Cooling Systems for Buildings

Addressed audience: solar thermal and heat pump researchers, building energy engineers, system designers and manufacturers

1. Introduction

With the urgent need to reduce greenhouse gas emissions, space heating and domestic hot water (DHW) for buildings, which account for around 15% of the European Union's total emissions (European Commission, 2020), must increasingly rely on heat pumps. The most common and cost-effective solution is the Air-Source Heat Pump (ASHP) system. A conceptually straightforward evolution consists in replacing its compact outdoor heat exchanger unit with a roof-mounted field of solar collectors that harvest heat from both ambient air and solar radiation (Kramer et al., 2023; Miglioli et al., 2023). Liquid-based photovoltaic-thermal (PVT) collectors can be both the sole heat source of the heat pump and electricity generators offsetting the compressor demand in a *single-source indirect-expansion PVT solar-assisted heat pump* (IDX-PVT-SAHP) system.

To operate efficiently at night on ambient heat alone, such collectors must be unglazed – designated Wind- and Infrared-Sensitive Collectors (WISC).

The system operates in contrasting regimes: at night the collector field acts as a large air-to-brine heat exchanger, while during the day solar irradiation raises the evaporator inlet temperature – improving the COP – or enables passive frost melting. Whether the IDX-PVT-SAHP outperforms the ASHP over a heating season depends on the balance between these two modes, and therefore on climate, collector characteristics, panel area, building demand and system configuration.

Despite growing interest, the literature presents systematic gaps. We could find no fully transparent and reproducible simulation model of such a system: published studies rely on proprietary platforms (TRNSYS, Polysun) with limited component-level disclosure. Results are confined to global annual metrics or monthly-averaged temperatures, without disaggregation by operating mode (Jaafar et al., 2022; Nielsen et al., 2024). Besides, Chhugani et al. (2023) include a parallel summer mode in which PVT heat feeds directly into the DHW tank, use a partially disclosed heat pump performance map, and apply a single frosting/defrosting-penalty assumption, all of which limit the understanding and generalisability of their ASHP comparison. Importantly, no study has yet demonstrated a clear seasonal performance advantage of a properly sized and installed IDX-PVT-SAHP over an ASHP system serving the same building, a gap explicitly noted by Kramer et al. (2023).

This paper takes a first step toward filling these gaps through (i) a fully-Python dynamic model following the architecture of TRNSYS Type 1286 (PVT), Type 402 (heat pump) and Type 88 (building), released as open source and therefore auditable; (ii) an operating-mode analysis of both the evaporator-to-ambient temperature pinch and the performance factor, which is the level at which the two heat sources genuinely differ; and (iii) a comparison of IDX-PVT-SAHP and ASHP under two explicit electrical boundaries and a continuous sweep of the frosting/defrosting penalty, so that the sensitivity of the ranking to those modelling choices can be read directly. The result is less a ranking than an identification of key modelling choices and opportunities for optimising the system.

2. Modelling

2.1 System description

As Fig. 1 shows, the system comprises: (a) a field of liquid-based WISC PVT collectors in a glycol/water primary loop which is the sole heat source of (b) a brine/water heat pump with an electric backup heater, (c) a hydronic space heating (SH) circuit controlling the indoor temperature of (d) the building, and (e) a domestic hot water (DHW) tank supplied exclusively by the heat pump condenser. Since brine/water heat pumps must have evaporator inlet temperature lower than a limit, there is a thermostatic valve at the outlet of the solar panels. PV electricity self-consumption offsets compressor demand or building load when simultaneous.

The ASHP system is the same system with an air-source heat pump instead of the brine/water heat pump supplied with a PVT collector field. The same area of photovoltaic (PV) panels is assumed as being installed as that of PVT panels, so this study focuses on the heat source alone.

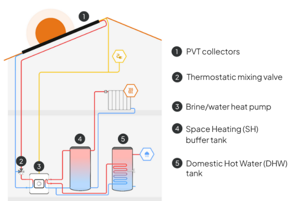

Fig. 1: Schematic of the IDX-PVT-SAHP system including an additional space heating buffer tank. In the present study, the heat pump condenser is directly connected to the hydronic space heating circuit.

2.2 Modelling framework and solution strategy

The model is implemented entirely in Python (NumPy/SciPy/pandas/pvlib), with no dependency on a commercial simulation environment. It is organised as independent component models – building, radiators, heat pump, PVT field – assembled by an *orchestrator* which manages the control logic. Four components deliberately mirror well-documented TRNSYS types so that results remain comparable with the literature: the building follows the single-capacitance formulation of Type 88, the ground coupling heat losses the calculation of Type 985, the heat pump the performance-map architecture of Type 402 (Transsolar, 2012), and the PVT collector the quasi-dynamic ISO 9806 formulation (ISO, 2025) used by Type 1286 (TESS, 2023).

The distinctive numerical feature of an IDX-PVT-SAHP is that source and sink are mutually dependent within a single time step: the heat extracted at the evaporator sets the collector fluid temperature, which sets the evaporator inlet temperature, which in turn sets the heat the compressor can extract. This loop is closed by a one-dimensional fixed-point problem on the mean collector temperature. All state variables are advanced from one step to the next, so the model is a genuine dynamic simulation. Any annual simulation below uses a 2-minute timestep, running in about 4 minutes on one core of a standard laptop.

The whole code base (component models, sizing rules, campaign driver and the analysis scripts that produce every figure and table of this paper) will be released as open source on GitHub by the end of 2026.

2.3 Building

All building characteristics, occupancy and appliance schedules are taken from the IEA SHC Task 44 / HPP Annex 38 reference framework (Dott et al., 2013), which defines the SFH15/SFH45/SFH100 family of single-family houses. SFH45 is considered here. The conditioned volume is represented by a single thermal capacitance C_b at uniform temperature T_b, in the manner of TRNSYS Type 88:

$$C_\mathrm{b}\frac{\mathrm{d}T_\mathrm{b}}{\mathrm{d}t} = \dot{Q}_\mathrm{transmission} + \dot{Q}_\mathrm{ventilation} + \dot{Q}_\mathrm{infiltration} - \dot{Q}_\mathrm{ground} + \dot{Q}_\mathrm{internal\ gains} + \dot{Q}_\mathrm{solar} \tag{1}$$

Envelope transmission uses a wind-dependent conductance, infiltration a fixed air change rate, and mechanical ventilation is set to zero. Ground coupling is not lumped into the envelope conductance but computed with the periodic ISO 13370 slab model fitted on the weather file itself, and solar gains are computed per glazed surface, each window carrying its own tilt and azimuth. Equation (1) is integrated implicitly, the step being closed by Picard iteration since emitter output and transmission losses both depend on the unknown T_b. Model equations and the full parameter set are given in the repository documentation.

2.4 Space heating circuit

Emitters are radiators modelled with two thermal nodes, the water content and the metal mass, the metal-to-air conductance being set at each iteration so that the converged solution satisfies the EN 442 characteristic $\dot{Q} = K_r\,\Delta T^{*n}$ exactly, with $n = 1.3$. This two-node structure is what makes the emitters dynamic: after a compressor stop the radiators keep releasing their stored energy, and after a start they absorb part of the delivered heat before the indoor air sees it.

Supply temperature follows a low-temperature heating curve $T_\mathrm{supply} = 45 - 0.75\,T_\mathrm{amb}$ [°C], and the circuit flow is adjusted to hold a 5 K temperature difference. A room thermostat switches the circuit with a ±0.5 K dead band, while the electric backup uses a tighter band, so that the heat pump alone completes the final approach to setpoint.

2.5 Domestic hot water demand

DHW demand is inspired by the IEA SHC Task 44 / HPP Annex 38 reference framework (Haller et al., 2013), from which the daily energy content, its seasonal variation and the draw temperature are taken (140 L/day at 45 °C on average), excluding the bath-tub and 55 °C-draw adaptations; the mains water temperature follows the Burch–Christensen correlation. The tank is not modelled but represented by an energy bucket charged at 50 °C with a 5 K rise over four production windows (07:00, 12:00, 15:00, 21:00, shares 20/10/40/30%), a deliberate simplification, sufficient here to capture heat pump performance under the correct temperature regimes.

2.6 Heat pump

Following the Type 402 architecture, the heat pump is described by two performance maps giving the condenser heat output and the compressor electrical input as functions of evaporator inlet temperature, condenser outlet temperature and relative compressor speed χ (between 0 and 1):

$$\dot{Q}_{\mathrm{HP,Cond}} = f_Q\left(\tilde{T}_{\mathrm{Eva,in}}, \tilde{T}_{\mathrm{Cond,out}}, \chi\right), \qquad P_{\mathrm{el,Comp}} = f_P\left(\tilde{T}_{\mathrm{Eva,in}}, \tilde{T}_{\mathrm{Cond,out}}, \chi\right), \qquad \tilde{T} = \frac{T\,[^\circ C]}{273.15} + 1 \tag{2}$$

Data sources. The brine/water unit is the ecoGEO$^+$ B/C 1-9, an inverter-driven R410A heat pump (EcoForest, 2024b) of which an R290 variant of similar performance exists; its operating points were supplied directly by the manufacturer and cross-checked against the public technical datasheets (Ecoforest Geotermia, S.L., 2024). The air/water reference is the ecoAIR$^+$ 1-9 PRO, inverter-driven on natural R290 refrigerant (EcoForest, 2024a), whose operating points come from that same datasheet document. The maps are fitted on the full operating-point dataset – 1 649 retained points over 26 ($T_{\mathrm{eva}}, T_{\mathrm{cond}}$) cells for the ecoGEO$^+$, 627 points over 12 cells for the ecoAIR$^+$. The two datasets do not cover the same domain: the ecoGEO$^+$ cells span evaporator inlet temperatures from −20 to +30 °C and condenser outlet temperatures from 35 to 65 °C, whereas the ecoAIR$^+$ cells form a complete 4×3 grid spanning only −15 to +7 °C on the evaporator side and 35 to 55 °C on the condenser side. Four interpolation methods were compared by leave-one-cell-out cross-validation; the cubic RBF, accurate to 0.11% MAPE on the condenser heat and 0.21% on the compressor power for the ecoGEO$^+$, is used throughout. Fig. 2 shows both fitted maps against the manufacturer points. This full disclosure of dataset and fitting procedure is what the reviewed literature lacks, and a prerequisite for the ASHP comparison.

The whole performance map (condenser heat and compressor power functions) of each heat pump is multiplied by a single capacity factor, chosen so that the heating thermal output at the design point equals the fraction of the design heat load prescribed in Section 2.9. Scaling the entire map changes the nominal power and leaves the shape of the performance surface, and with it the COP, unchanged.

Operating constraints and control. Three constraints are enforced on top of the maps: the operating point must lie inside the manufacturer's compressor envelope, the modulation bounds are interpolated from the manufacturer grid, and speed changes are rate-limited. In space heating the flow rate and supply temperature are imposed by the emitter circuit and the compressor speed is the unknown, found by Brent's method; in DHW service the logic is reversed, the speed being imposed (0.75 in winter, 0.45 in summer) along with the tank supply temperature and the temperature rise (5 K), and the condenser flow rate deduced. The heat extracted at the evaporator, which closes the coupling with the collector field, is $\dot{Q}_{\mathrm{HP,Eva}} = \dot{Q}_{\mathrm{HP,Cond}} - \eta_{\mathrm{HP}} P_{\mathrm{el,HP}}$ with $\eta_{\mathrm{HP}} = 0.9$. The same component serves the air-source reference: switching the system type replaces the whole source loop by $T_{\mathrm{HP,Eva,in}} = T_{\mathrm{amb}}$ and loads the ecoAIR$^+$ maps, everything else unchanged.

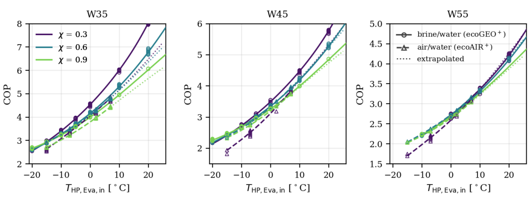

Fig. 2: COP of both heat pumps versus evaporator inlet temperature, at three condenser outlet temperatures and three compressor speeds. Lines are the cubic RBF maps, markers the manufacturer points (Ecoforest Geotermia, S.L., 2024): ecoGEO$^+$ solid with circles, ecoAIR$^+$ dashed with triangles, dotted beyond its last measured point (7 °C).

Frosting/defrosting penalty. PVT panels are assumed to require no defrost cycle, as supported by the field evidence of Leibfried et al. (2018) for this fin spacing. For the ASHP, certification points are supposed to include frosting/defrosting, but manufacturer data generally do not. Thus, frosting/defrosting is modelled as a COP reduction depending on outdoor temperature and relative humidity, using the experimental penalty curve based on measurements at ISFH and published in Chhugani et al. (2023) (their Fig. 3b). The COP multiplier is split between the two maps so that the loss is shared between reduced capacity and increased power. It is applied inside them before the speed search, so that the controller compensates the degradation. This curve is the anchor of the sensitivity study: it was measured on a different heat pump and its transposability is not established. Six further multiples of it are swept, on a regular grid from no penalty at all to 3× the curve as measured.

2.7 PVT collector field and source loop

Unglazed WISC collectors are modelled as a single thermal node at mean fluid temperature $T_{\mathrm{PVT,m}}$, following the quasi-dynamic formulation of ISO 9806 (ISO, 2025). The net specific gain of the absorber is:

$$\dot{Q}_{\mathrm{PVT}} = \underbrace{\eta_{\mathrm{b}}\, G_{\mathrm{b}} + \eta_{\mathrm{d}}\, G_{\mathrm{d}}}_{\text{optical}} - \underbrace{(b_1 + a_3 u)\left(T_{\mathrm{PVT,m}} - T_{\mathrm{amb}}\right)}_{\text{convection}} - \underbrace{a_4\, \sigma \left(T_{\mathrm{amb}}^4 - T_{\mathrm{sky}}^4\right)}_{\text{long-wave}} - \underbrace{a_5 \frac{\mathrm{d}T_{\mathrm{PVT,m}}}{\mathrm{d}t}}_{\text{capacitance}} \tag{3}$$

with wind-dependent optical efficiencies $\eta_{\mathrm{b}} = \eta_{0,\mathrm{b}} K_{\mathrm{b}}(\theta_{\mathrm{L}}, \theta_{\mathrm{T}}) - a_6\,(u - 3)$ for the beam component and $\eta_{\mathrm{d}} = \eta_{0,\mathrm{b}} K_{\mathrm{d}} - a_6\,(u - 3)$ for the diffuse one. The wind-dependent loss coefficient, the wind-dependent optical efficiency and the explicit long-wave term are key factors in WISC collector behaviour. The capacitance term a_5 models transient behaviour. The source balance further accounts for the circulator heat input and for the outdoor pipe losses.

In the present study, the PVT collectors are Dualsun SPRING MAX panels[1] (Dualsun, 2024), tilted at 45° and facing south. Their certified SolarKeymark coefficients are: $A_{\mathrm{G}} = 1.95\ \mathrm{m}^2$, $\eta_{0,\mathrm{b}} = 0.376$, $K_{\mathrm{d}} = 0.98$, $b_1 = 15.454\ \mathrm{W\,m^{-2}K^{-1}}$, $a_3 = 7.162\ \mathrm{J\,m^{-3}K^{-1}}$, $a_5 = 28\,870\ \mathrm{J\,m^{-2}K^{-1}}$ and $a_6 = 0.045\ \mathrm{s\,m^{-1}}$. The long-wave factor a_4, not certified, is set to 0.40, in line with its design (heat exchanger attached to the photovoltaic panel), experimental data obtained from heat pump coupling, and the recommendations set out in the ISO9806 standard.

Source-loop auxiliaries and the electrical boundary. The brine loop is operated at a constant 120 L/h per panel, so the field flow rate scales with the number of panels and each collector always sees the same specific flow. It needs a circulator, an auxiliary the air/water heat pump does not have. This study assumes an average 80 W of electrical consumption over heat pump compressor operation, of which 20 W are dissipated into the brine. These operating figures are consistent with those of a variable-speed circulator of the Grundfos UPML class. That consumed energy is referred to as E_{PVTpump}. For the air/water unit the counterpart is the fan, which the manufacturer figures are assumed to include, as EN 14511 prescribes.

Thermostatic mixing valve. Brine/water heat pumps require the evaporator inlet to stay below a manufacturer limit $T_{\max} = 30\,°\mathrm{C}$. A three-way valve therefore mixes the panel return with the colder evaporator outlet, the mixing ratio α being the fraction of the source flow actually passing through the collectors, resolved on the current evaporator outlet so that the valve position remains sensitive to compressor speed. When the limit cannot be held even at minimum panel flow, the heat pump is stopped for that step, a summer failure mode specific to this system, which does not occur in any of the runs reported here.

2.8 Control and system operation

Component models are assembled by an orchestrator applying strict DHW priority, with a single intermediate step separating DHW from space heating so that the condenser circuit is never switched from the tank to the radiators within one step. When neither service is called the solver still runs at zero flow: the collectors keep exchanging with sun, sky and air, stagnating in sunshine and relaxing towards ambient at night, and this evolution sets the source temperature available at the next start.

[1] *SPRING4 425 TOPCon Finned*

2.9 Sizing rules

Comparing two heat-generation technologies is only meaningful if both are sized by the same explicit rules, applied automatically to every configuration. A Typical Meteorological Year smooths cold spells and is unsuitable for sizing, so the design outdoor temperature is the NF EN 12831 base temperature, resolved from the site coordinates and corrected for altitude: -15 °C for Strasbourg, against a TMY minimum of -9.9 °C. The design load excludes all gains, per the same standard, and amounts to 5.60 kW here. Four rules follow. The **heat pump** is rated at 80% of the peak load, per the DTU 65.16 range of 0.8–1.2, the balance being covered by the electric backup. The **emitters** are calibrated numerically on the steady solution of the actual emitter model so that the circuit delivers 1.2 times the design load at the base temperature with 6 radiators on the heating curve, broadly in line with the 1.3× recommendation of Task 44 (Haller et al., 2013). The **PVT field** is sized proportionally to the heat pump capacity at B0/W35, at 1.5 panels per kW, as recommended by Dualsun for this architecture. The **backup** is rated at 1.0 times the design load, so that it can cover the full load if the heat pump is unavailable.

Regarding the heat pump sizing, the capacity factor applied to the whole performance map, as described in Section 2.6, is then 0.600 for the ecoGEO^{+} (rated at $-20/56.2\,°\mathrm{C}$, the evaporator inlet being estimated at 5 K below ambient at the design point) and 0.934 for the ecoAIR^{+} (rated at $-15/56.2\,°\mathrm{C}$). The two rescaled heat pumps deliver 7.68 kW at B0/W35 and 7.59 kW at A2/W35 respectively.

2.10 Weather data and pre-processing

The reference climate is the PVGIS typical meteorological year at the site coordinates, upsampled to the 2-minute step: state variables linearly, solar components by a monotone interpolation of *cumulative energy*, which preserves the hourly totals and avoids the spurious peaks of interpolating the fluxes directly. Horizontal components are transposed to the collector plane, beam by the cosine of the incidence angle and sky diffuse by Perez, the same routine serving the building glazing so that both see consistent solar gains. For the collector loss term, the 10 m wind is halved to account for roof height and sheltering, as recommended in Task 44 (Haller et al., 2013).

3. Methodology

3.1 Simulation campaigns

Two questions drive the study, and one parametric campaign answers each. Both share the same climate, building, emitters, controls and automatic sizing rules (see 2.9); only the swept quantity changes, so any difference in the results can only come from that quantity.

(i) How much does the IDX-PVT-SAHP depend on collector area? The PVT field is swept from 8 to 18 panels, alongside the size returned by the automatic sizing rule, 12 panels here. Since the field is the sole heat source, for the PVT design under study (Dualsun SPRING MAX), its area sets the temperature at which heat reaches the evaporator.

(ii) How does it compare with an air-source heat pump, given that the comparison hinges on an uncertain frosting/defrosting penalty? The ASHP is run across seven factors applied to the ISFH-measured frosting/defrosting penalty curve of 2.6, regularly spaced from 0× to 3× in steps of 0.5. Sweeping lets the comparison be summarised by the penalty at which the two systems become equivalent.

A configuration is retained only if it delivers the service in full. The 12-panel configuration is called the **reference IDX-PVT-SAHP** throughout, and the **reference ASHP** denotes the air/water system at 1.5× the ISFH-measured frosting/defrosting penalty.

3.2 Performance indicators and evaporator-to-ambient temperature pinch

The Coefficient of Performance (COP) given in manufacturer data is an *instantaneous* ratio: the condenser thermal power divided by the electrical power $P_{\mathrm{el,HP}}$ the unit draws at that operating point, which per EN 14511 covers the compressor, the control and power electronics, and the shares of the condenser- and evaporator-side circulators attributable to those two heat exchangers alone, or, for an air/water unit, its fan.

Integrated over any subset of the year (one service, one period, one outdoor-temperature class), the same quantity is called *performance factor* (PF); over a full year it becomes a seasonal performance factor (SPF). Two labels indicate what is counted as delivered heat, and how far the electrical boundary extends.

On the numerator, bSt (*before storage*) counts all the heat delivered at the condenser, $Q_{\mathrm{HP,Cond}}$; SHP counts the *useful* energy: Q_{SH} released by the radiators into the building plus $Q_{\mathrm{DHW,use}}$ actually drawn, and therefore charges the storage losses to the system. On the denominator, three nested boundaries are used, following Miara et al. (2014): $0^{\oslash}$ is E_{HP} as just defined, the heat pump as the standards delimit it; $1^{\oslash}$ adds the source-side circulator consumption attributable to the PVT loop pressure drop, E_{PVTpump}; and $2^{\oslash}$ adds the backup heater, E_{heater}. For the air/water unit $1^{\oslash}$ and $0^{\oslash}$ coincide because it has no source loop and its fan is already inside E_{HP}. The headline indicator of this paper is:

$$\mathrm{SPF}_{2^{\oslash},\mathrm{SHP}} = \frac{Q_{\mathrm{SH}} + Q_{\mathrm{DHW,use}}}{E_{\mathrm{HP}} + E_{\mathrm{PVTpump}} + E_{\mathrm{heater}}}. \tag{4}$$

This metric is equivalent to $\mathrm{SPF}_{\mathrm{SHP}}$ defined in Malenkovic et al. (2013) because this reference accounts for the electric consumption of the circulation pump dedicated to the loop between the condenser and the hot buffer tank which is nearly included in E_{HP} here (pressure drops occur mainly in the condenser). The SPF_{4+} of Hadorn (2015) shares the numerator but also includes the electric consumption of the sink-side circulation pump attributable to the space heating circuit pressure drop.

Finally, IDX-PVT-SAHP systems should be compared through the temperature penalty each concedes in order to extract heat from the PVT panels to the evaporator, the *pinch* $T_{\mathrm{HP,Eva,in}} - T_{\mathrm{amb}}$. Pinch averages are weighted by the evaporator heat $Q_{\mathrm{HP,Eva}}$, the quantity conjugate to it in the source energy balance. This pinch does not exist for an air-source heat pump which is modelled here via a performance map evaluated at the outdoor temperature i.e. the air inlet temperature of the outdoor air/refrigerant heat exchanger.

4. Results

4.1 Thermal comfort, delivered energy and backup use

Every configuration compared below delivers the same service, which is the condition that makes the electricity figures comparable. Across the thirteen configurations (six PVT field sizes and seven frosting scenarios) the delivered space heating spans 0.09% and the drawn hot water 0.01%, and thermal comfort is met in all of them: the indoor temperature never falls below 19.3 °C against a threshold of $\hat{T}_{\mathrm{indoor}} - 1 = 19.0$ °C. The space heating delivered energy is about 42.4 kWh/m^2/y, which is consistent with the SFH45 reference building from the Task 44 framework (46.3 kWh/m^2/y for a different Strasbourg's TMY dataset). The DHW delivered energy is 1826 kWh/y with total losses of 142 kWh/y or 7.2% of production.

The electric backup is negligible in all cases: 2.7 kWh/y, i.e. 0.11% of total electricity. This is a consequence of the sizing and control rules: the heat pump is sized at 0.8× the design load at $T_{\mathrm{design}} = -15$ °C, while the TMY minimum is −9.9 °C, so the heat pump alone holds the water-law setpoint on 97% of the steps where it runs to heat the building. On the few steps it misses, the shortfall is 1.2 K at the median and the compressor is at full speed on only a third of them: most misses are transients, not a lack of capacity. The backup is released only when the setpoint is missed and the compressor is saturated, a conjunction that occurs on 0.04% of the year. The backup is thus not a differentiating factor between the systems here, and the comparison rests entirely on compressor efficiency.

4.2 Evaporator-to-ambient temperature pinch

Evaporator-extracted-energy-weighted averages of $T_{\mathrm{HP,Eva,in}} - T_{\mathrm{amb}}$ are taken over all heat pump operation, either in 1 K outdoor-temperature bins for Fig. 3, or over the whole year for the operating modes averages quoted below. Every bin is plotted whatever its weight, its population being shown by the marker area and by the operating-hours band. Start-up transients are kept: on the first steps of a cycle the loop still holds fluid warmed while the panels were stagnating, and that heat is genuinely drawn by the heat pump.

Night-time pinch. At night the pinch is markedly negative, −5.2 K for space heating in the reference configuration, and enlarging the PVT field shallows it monotonically and sublinearly, from −7.1 K at 8 panels to −3.8 K at 18: the first four panels beyond eight recover 1.9 K, the four beyond twelve only 1.0 K. The profile has three zones. Over the central band, −4 to +12 °C and 93% of the night-time evaporator heat, the pinch rises almost affinely by +0.293 K/K (R^2 = 0.99 on the bin means), +3.8 K in all; a step-by-step regression weighted by the evaporator heat attributes +1.3 K to the shrinking sky-to-ambient difference and +1.0 K to the rising wind. Below −4 °C the branch steps upwards by 1.4 K, due to higher average wind speeds, on 34 operating hours carrying 2.5% of the night-time evaporator heat. Above 12 °C, where operation is DHW only at fixed compressor speed, it flattens to about −2.6 K.

Day-time pinch. During the day, absorbed solar irradiation warms the absorber and raises the source temperature: the pinch narrows to −2.5 K for space heating and reverses to +2.6 K for DHW, mostly thanks to mid-season and summer daytime periods with higher levels of solar radiation and stagnation between cycles. The profile has the same three-zone structure. It rises affinely from 0 to 20 °C (+0.44 K/K, R^2 = 0.95) as irradiance grows and both the sky-to-ambient temperature difference and the evaporator draw shrink. It reverses below 0 °C, where cold hours in this climate are almost all clear-sky ones and a field tilted at 45° meets the low winter sun almost head-on, recovering 2.1 K on average from −4.7 K at +0.5 °C (on 3.9% of the daytime evaporator heat). It falls above 20 °C, where the mixing valve caps the evaporator inlet at T_{max} = 30 °C, making the pinch simply 30 °C − T_{amb}, a limit of the heat pump and not a degradation of the collector.

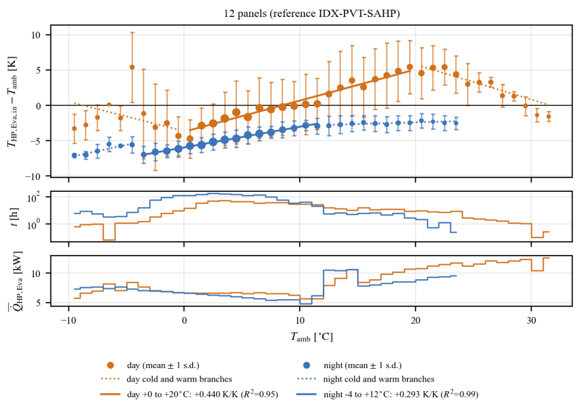

Fig. 3: Evaporator inlet pinch $T_{HP,Eva,in} - T_{amb}$ versus outdoor temperature for the recommended PVT field (12 panels), in 1 K bins weighted by the evaporator heat. Error bars are one standard deviation of the distribution, not a confidence interval; marker area scales with bin population; the middle and bottom bands give operating hours (log scale) and mean evaporator power per bin. Solid lines are the weighted fits over the central band, dotted ones over the cold and warm branches. No bin is filtered out.

4.3 Operating-mode performance factors comparison

Where each system wins. Tab. 1 and Fig. 4 compare the reference IDX-PVT-SAHP (12 panels) with the reference ASHP (1.5× the ISFH penalty), broken down by service (space heating or DHW) and by daylight, read first at the $0^{\oslash}$ boundary (the heat pump alone), which isolates the quality of the heat source.

At that boundary the PVT source is strongest whenever irradiation contributes: +9.9% on daytime space heating and +8.5% on daytime DHW. At night it keeps a thin margin on space heating, +2.6%, and loses it on DHW, −0.7%. Fig. 4 resolves the same comparison against outdoor temperature and separates the two mechanisms: below 0 °C the PVT curve sits below the air-source curve on three of the four operating modes, by 4.2% on night-time space heating which is where most of that electricity is spent, the radiative loss to the sky outweighing a frosting penalty that stays mild in dry cold air. The ranking reverses just above 0 °C: between 0 and +5 °C the PVT source gains 4.7% on night-time and 8.5% on daytime space heating, frosting biting hardest there while the collector receives some irradiance.

The seasonal performance factor of each operation mode is exactly the average of the subset factors weighted by the electricity each consumes, which is why the lower panel of Fig. 4 carries the compressor electricity per bin. The bins below 0 °C, where the PVT source loses, take 24% of that electricity, against 44% between 0 and 5 °C where it gains most. Across operating modes the weighting works the other way: night-time space heating alone consumes 65% of the compressor electricity against 12% for daytime space heating, so the daytime advantage may not be enough to really outperform the ASHP system. Over the year the compressor of the IDX-PVT-SAHP draws 2265 kWh against 2358 kWh for the reference ASHP, 3.9% less.

What the source hydraulics cost. That comparison leaves out an auxiliary the PVT field requires and the air/water heat pump does not. Charging the source-loop circulator (80 W whenever the compressor runs, 178 kWh/y) moves every PVT performance factor down by 0.16 to 0.39, by 0.25 on average over the four operating modes, while leaving the air/water figures untouched. The $1^{\varnothing}$ block of Tab. 1 is therefore the narrowest boundary at which the two systems compare like with like, and it shows what remains of the advantage: +2.0% on daytime DHW, parity within 1% on daytime space heating, and deficits of 4.9% and 5.8% on the two night-time services. A single auxiliary drawing 7% of the heat pump electricity is thus enough to cancel a source advantage of comparable size. Sizing the brine loop for the lowest achievable pressure drop, in the PVT collector exchangers as much as in the pipework and hydraulic components, is therefore not an installation detail but a condition for the architecture to deliver what its source is worth.

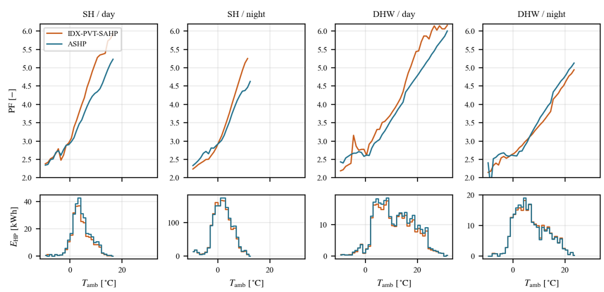

Fig. 4: Performance factor per outdoor-temperature bin (top) and compressor electricity per bin (bottom), reference IDX-PVT-SAHP against reference ASHP, by service and daylight. A difference in performance factor moves the seasonal factor only in proportion to the electricity spent in that bin.

Tab. 1: Electricity-weighted performance factor per operating mode, reference IDX-PVT-SAHP against reference ASHP. $0^{\varnothing}$ is the heat pump alone and isolates the source; $1^{\varnothing}$ adds the source-loop circulator, which the air/water unit does not have, so only $1^{\varnothing}$ compares like with like. The last column is the share of the annual $1^{\varnothing}$ electricity spent in that operating mode, which is the weight it carries in the seasonal factor. Pinch is that of the IDX-PVT-SAHP.

Service	Period	$PF_{0^{\varnothing},bSt}$			$PF_{1^{\varnothing},bSt}$			Pinch	Share of
		IDX-PVT	ASHP	Δ	IDX-PVT	ASHP	Δ	K	$E_{1^{\varnothing}}$
SH	day	3.92	3.57	+9.9%	3.54	3.57	−1.0%	-2.5	12%
SH	night	3.30	3.22	+2.6%	3.06	3.22	−4.9%	-5.2	65%
DHW	day	4.12	3.80	+8.5%	3.87	3.80	+2.0%	+2.6	13%
DHW	night	3.22	3.24	−0.7%	3.05	3.24	−5.8%	-3.6	10%

4.4 Sensitivity of seasonal performance factors on frosting/defrosting penalty

Tab. 2 and Fig. 5 benchmark the reference IDX-PVT-SAHP (12 panels) against the ASHP across the seven frosting scenarios, regularly spaced from no penalty at all to 3× the ISFH-measured curve. Since both systems deliver the same service, the comparison is stated as the annual electricity $E_{2^{\varnothing}} = E_{HP} + E_{heater} + E_{PVTpump}$ the IDX-PVT-SAHP saves, or costs, relative to each scenario. It draws 2445 kWh/y, of which 178 kWh/y for the source-loop circulator, for a seasonal factor of 3.17.

For the recommended field of 12 PVT panels the penalty at which the two systems become equivalent is 1.99× the ISFH frosting/defrosting penalty curve, below it the air source draws less electricity, above it the PVT source does. Collector area lowers the bar, from 2.48× at 8 panels to 1.59× at 18, with the same decelerating returns as the evaporator-to-ambient temperature pinch.

Whether a factor near two is plausible is the question on which the comparison turns, and it cannot be settled here: the ISFH curve is the only detailed, experimentally grounded map of the effect we could find, but it was measured on another heat pump and its transposability is not established. That is precisely why the sweep, rather than any single scenario, is what this section reports.

The seven scenarios span 526 kWh/y, while the PVT-loop circulator alone accounts for 178 kWh/y, as much as a swing of one unit in the penalty factor. On this system, how this pump is modelled and counted matters nearly as much as which frosting/defrosting model is adopted, and both deserve to be stated explicitly in any comparative assessment.

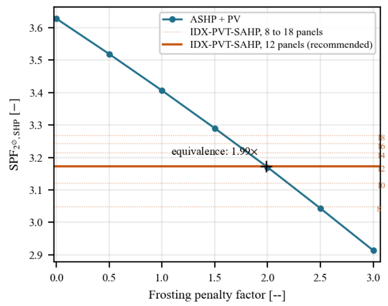

Fig. 5: $SPF_{2\oslash,SHP}$ of the ASHP versus frosting/defrosting penalty factor, against the levels reached by the IDX-PVT-SAHP from 8 to 18 panels (reference, 12 panels, solid; other sizes dotted). The cross marks equivalence.

Tab. 2: Seasonal performance factor $SPF_{2\oslash,SHP}$ (Eq. 4) and total annual electricity $E_{2\oslash}$ of the reference IDX-PVT-SAHP and of the ASHP under the seven frosting scenarios swept. $\Delta E_{2\oslash}$ is the electricity the IDX-PVT-SAHP saves relative to that scenario; negative means it draws more.

Scenario	$SPF_{2\oslash,SHP}$ –	$E_{2\oslash}$ kWh/y	$\Delta E_{2\oslash}$ kWh/y (%)	Scenario	$SPF_{2\oslash,SHP}$ –	$E_{2\oslash}$ kWh/y	$\Delta E_{2\oslash}$ kWh/y (%)
No penalty	3.63	2139	−306 (−14.3%)	2×	3.17	2448	+3 (+0.1%)
0.5×	3.52	2205	−240 (−10.9%)	2.5×	3.04	2550	+105 (+4.1%)
1×, ISFH curve	3.41	2278	−167 (−7.3%)	3×	2.91	2665	+220 (+8.2%)
1.5×	3.29	2358	−86 (−3.7%)				

5. Discussion

Putting the margin in perspective. Across the whole sweep the two systems stay within a few per cent of one another, which matters because the choice between them may rest on factors beyond performance: the PVT option removes the outdoor fan unit (its bulk, visual impact and acoustic emissions are often the binding constraint in dense urban settings) with no borehole drilling, and it installs a large photovoltaic area in the same operation. The relevant question is then what efficiency difference those advantages are worth.

An upper bound the present control does not reach. The shortfall reported above is not a verdict on the concept, because neither the control nor the hydraulics exploit what the pinch analysis reveals. Two first-order estimates size what is being left on the table. Shifting two thirds of the night-time space-heating output into daylight hours with a hot-side buffer (the daytime performance factor for space heating being 3.54 against 3.06 at night) may save 142 kWh/y and raise the seasonal factor from 3.17 to 3.37, above the reference ASHP at 3.29. This estimate rests on one assumption that the model does not verify: charging a buffer tank above the emitter temperature costs COP, and that is assumed to be offset by concentrating production in the sunniest hours. Whether the two cancel is precisely what a control study would have to establish, and until it does the figure is an upper bound. Letting the PVT field pre-heat the DHW tank directly, as a solar loop bypassing the heat pump, could save about 250 kWh/y of electricity consumption. Together the two would reach $SPF_{2\oslash,SHP} \approx 3.7$, above the air-source system in every frosting/defrosting penalty scenario of the sweep. Both are estimates, not simulation results: they size an opportunity and are the reason the concept deserves hydraulic variants (e.g., hot buffer tank for space heating and heat pump bypass) and specific control strategies (e.g., optimal scheduling with weather data), both numerically and experimentally.

Frosting of the PVT collectors. One asymmetry deserves to be stated explicitly: the frosting/defrosting penalty is applied to the air-source unit only, while the PVT field is assumed never to need one. The field evidence of Leibfried et al. (2018) supports that assumption over the range explored here, but it is not unconditional. Frost forms when the PVT collector is below the dew point and 0 °C, met on 1 077 of the 2 219 annual compressor-operating hours (49%) at +1.6 °C average. It can reduce the heat gain by about 5-15%, depending on the thickness of the frost layer. The conditions for a necessary defrost cycle, its control, duration and energy cost should be quantified by a specific experimental study. The model also ignores the potential latent-heat gain of condensation and frost formation, the sensible contribution of rain, and snow cover.

Beyond energy. The natural continuation is an economic and environmental assessment, which the energy results alone cannot settle. Such an analysis would also reframe the sizing question, and the choice of a collector with a better wind and infrared response rather than more of the same one.

6. Conclusions

A transparent, fully-Python dynamic model for IDX-PVT-SAHP and ASHP systems, with fully disclosed component models, manufacturer performance maps and automatic sizing rules, has been applied to a single-family house SFH45 in Strasbourg, both systems delivering an identical service ($\approx$ 42.4 kWh/m^2/y of space heating and $\approx$ 1830 kWh/y of drawn hot water) at full thermal comfort and with negligible electric backup.

The operating-mode-resolved analysis is the substantive result. At the compressor the PVT source is superior whenever irradiation contributes, by 9.9% on daytime space heating and 8.5% on daytime DHW, and concedes a pinch of -5.2 K at night, governed by the sky-to-ambient temperature difference and the wind. Because night-time space heating alone consumes 65% of the electricity, that daytime advantage may not be enough to really outperform the air-source system.

The seasonal performance comparison then turns on two modelling and accounting choices. When charging the source-loop circulator the PVT field requires, 178 kWh/y, the reference IDX-PVT-SAHP system (12 panels) costs more than the ASHP system below a frosting/defrosting penalty of 1.99× the ISFH curve, the threshold at which the two systems become equivalent. That single auxiliary weighs as much as a swing of one unit in the penalty factor, so how the PVT circulator is modelled matters nearly as much as which air-source heat pump frosting/defrosting model is adopted. It also makes the hydraulic design of the PVT loop a lever in its own right: minimising the pressure drop of the evaporator, the piping and the hydraulic components directly reduces the only auxiliary the air-source system does not carry.

These figures are orders of magnitude produced by a transparent model, not a verdict. The sensitivity sweep is reported precisely because the frosting/defrosting penalty for ASHP, which decides the ranking, rests on a single published curve measured on another heat pump. Settling the comparison would require heat pump performance maps and frosting/defrosting behaviour measured independently, ideally from a parallel experimental campaign running both systems on the same building, weather and demand. The model presented here makes the operating-mode level diagnosis possible and provides the basis on which optimised hydraulic configuration and control strategies (shifting production into daylight hours, and letting the collectors feed the DHW tank directly) can be designed and quantified. Those two strategies are not marginal: first-order estimates put their combined effect at $SPF_{2\oslash,SHP} \approx 3.7$ against 3.17 here, which would place the IDX-PVT-SAHP above the air-source system under every scenario considered (saving 11% of electric consumption relatively to the reference ASHP system).

Use of LLM assistance. The simulation code and this manuscript were developed with the assistance of Claude Code (Anthropic, model Opus 5), used as a pair-programming tool, mainly to structure and verify the model, and as a drafting aid, under continuous author supervision; all modelling choices, assumptions, results and conclusions are the authors' own and were verified against the source data. The assistant produced about 10 million output tokens, roughly 20 kgCO_2eq for the whole project at an order of magnitude of 2 mgCO_2eq per token. At the $\approx$ 40 gCO_2eq/kWh of the French grid over 2020–2025, that equals 21% of the annual emissions of one reference air-source system studied here, or about ten weeks of it. That seems acceptable against the help it gave on key choices in energy-efficiency renovation. But beyond carbon, the development and use of non-local heavy LLMs should be limited for reasons of land use, water and electricity consumption, and concentration of informational power.

7. References

Chhugani, B., Pärisch, P., Helmling, S., Giovannetti, F., 2023. Comparison of PVT – heat pump systems with reference systems for the energy supply of a single-family house. Solar Energy Advances 3, 100031. doi:10.1016/j.seja.2022.100031.

Dott, R., Haller, M., Ruschenburg, J., Ochs, F., Bony, J., 2013. The reference framework for system simulations of the IEA SHC Task 44 / HPP Annex 38, Part B: Buildings and space heat load. Technical Report. SPF Institut für Solartechnik, HSR. Rapperswil, Switzerland. Report C1 Part B.

Dualsun, 2024. SPRING MAX – technical datasheet. URL: https://dualsun.com/en/professionals/datasheet/spring4-425-topcon-finned/. accessed: 2025.

EcoForest, 2024a. EcoAir Pro 1-9 air/water heat pump – technical documentation. URL: https://downloads.ecoforest.com/en/productos/ecoair-pro-1-9/. accessed: 2025.

EcoForest, 2024b. EcoGeo 1-9 brine/water heat pump – technical documentation. URL: https://downloads.ecoforest.com/en/productos/ecogeo-1-9/. accessed: 2025.

Ecoforest Geotermia, S.L., 2024. Technical datasheets – heat pumps. URL: https://www.ecoforest.com. includes the ecoGEO$^+$ B/C 1-9 brine/water unit (inverter, R410A) and the ecoAIR$^+$ 1-9 PRO air/water unit (inverter, natural R290 refrigerant). Accessed: 2025.

European Commission, 2020. A Renovation Wave for Europe – Greening our buildings, creating jobs, improving lives. Technical Report. European Commission. COM(2020) 662 final.

Hadorn, J.C. (Ed.), 2015. Solar and Heat Pump Systems for Residential Buildings. 1st ed., Ernst & Sohn, Berlin. doi:10.1002/9783433604830.

Haller, M., Dott, R., Ruschenburg, J., Ochs, F., Bony, J., 2013. The reference framework for system simulations of the IEA SHC Task 44 / HPP Annex 38, Part A: General simulation boundary conditions. Technical Report. SPF Institut für Solartechnik, HSR. Rapperswil, Switzerland. Report C1 Part A, final revised 07.03.2013.

ISO, 2025. ISO 9806:2025 solar energy – solar thermal collectors – test methods. URL: https://www.iso.org/standard/78801.html.

Jaafar, M., Chhugani, B., Brottier, L., 2022. Numerical study of the effect of hybrid solar collectors on the performances of the system combining PVT with heat pumps, in: Proceedings of EuroSun 2022 – ISES and IEA SHC International Conference on Solar Energy for Buildings and Industry, Kassel, Germany. pp. 1–8. doi:10.18086/eurosun.2022.08.06.

Kramer, K., Mehnert, S., Hausner, R., Mugnier, D., Häberle, A., 2023. Photovoltaic thermal technology: collectors, systems, and applications. Energy Technology 11, 2300378. doi:10.1002/ente.202300378.

Leibfried, D., Wagner, A., Abdul-Zahra, A., 2018. Final report on the Solink funding project – Highly efficient heat supply for existing and new buildings based on the intelligent combination of PVT and heat pump technology – Part 1: Function development and setting up a user consortium. Technical Report 33226/01. German Federal Environmental Foundation.

Malenkovic, I., Pärisch, P., Eicher, S., Thür, A., Dott, R., Carbonell, D., 2013. Definition of main system boundaries and performance figures for reporting on SHP systems. Technical Report. IEA SHC Task 44 / HPP Annex 38. Deliverable B1.

Miara, M., Günther, D., Langner, R., Helmling, S., 2014. Efficiency of heat pumps in real operating conditions. Technical Report. Fraunhofer Institute for Solar Energy Systems ISE. Freiburg, Germany.

Miglioli, A., Aste, N., Del Pero, C., Leonforte, F., 2023. Photovoltaic-thermal solar-assisted heat pump systems for building applications: integration and design methods. Energy and Built Environment 4, 39–56. doi:10.1016/j.enbenv.2021.07.002.

Nielsen, E., Dragsted, J., Perers, B., Furbo, S., Dannemand, M., 2024. How does the thermal characteristics of PVT panels influence the performance of PVT heat pump systems, in: Proceedings of EuroSun 2024 – ISES and IEA SHC International Conference on Sustainable and Solar Energy for Buildings and Industry, Limassol, Cyprus. doi:10.18086/eurosun.2024.07.15.

TESS, 2023. TRNSYS TESS Libraries – General descriptions, version 18. Thermal Energy System Specialists. URL: https://www.trnsys.com/tess-libraries/GeneralDescriptions_TESSLibs18.pdf.

Transsolar, 2012. TRNSYS Type 402 – Detailed heat pump model using a performance map. Transsolar. URL: https://trnsys.de/static/21bb1ffeb7137ab7f36bda0f863814be/Type_402_manual.pdf.